

T. WATANABE¹
H. WATAKABE¹
T. SAMESHIMA^{1,✉}
M. MIYASAKA²

Electrical properties of solid-phase crystallized polycrystalline silicon films

¹ Tokyo University of Agriculture and Technology, 2-24-16 Nakacho, Koganei, Tokyo 184-8588, Japan
² Seiko Epson Corporation, Nagano 392-8502, Japan

Received: 21 May 2002/Accepted: 10 June 2002
Published online: 4 December 2002 • © Springer-Verlag 2002

ABSTRACT Analyses of free-carrier optical absorption and Hall-effect current measurements indicated in high carrier mobilities of $32 \text{ cm}^2/\text{Vs}$ and $30 \text{ cm}^2/\text{Vs}$, respectively, and low carrier densities of $5.0 \times 10^{19} \text{ cm}^{-3}$ and $3.8 \times 10^{19} \text{ cm}^{-3}$, respectively, for $1.1 \times 10^{20} \text{ cm}^{-3}$ -phosphorus-doped solid-phase crystallized polycrystalline silicon films fabricated at 600°C for 48 h. The silicon films had good crystalline properties of the crystalline grains and a low crystalline volume fraction of 0.43. A XeCl excimer laser anneal at $500 \text{ mJ}/\text{cm}^2$ effectively increased the carrier density to $1.1 \times 10^{20} \text{ cm}^{-3}$, and also increased the crystalline volume fraction to 0.93. Moreover, H_2O -vapor heat treatment at $1.3 \times 10^6 \text{ Pa}$ for 3 h at 260°C reduced the density of the defect states from $6.2 \times 10^{18} \text{ cm}^{-3}$ to $2.6 \times 10^{18} \text{ cm}^{-3}$.

PACS 73.20.Hb; 74.25.Fy; 61.72.Tt; 61.72.Bb

1 Introduction

Solid-phase crystallized polycrystalline silicon (SPC-poly-Si) films have been widely used for electrical devices such as thin-film transistors (TFTs). The growth mechanism and structural properties of SPC-poly-Si films have been investigated using transmission electron microscopy and X-ray-diffraction measurements. From these studies, SPC-poly-Si films are understood to be dendritic crystalline grains of about $\sim \mu\text{m}$ size, having many defects within the crystalline grains [1–6]. For reduction of defects in SPC-poly-Si films, an excimer laser anneal has been carried out [6]. However, electrical properties of SPC-poly-Si films are not well understood by comparison with structural properties.

In this paper, we report electrical and structural properties of SPC-poly-Si films and their improvement. The crystalline grain and grain-boundary properties are investigated using analysis of free-carrier optical absorption (FCA) and Hall-effect current measurements. We carried out a XeCl excimer laser anneal and high-pressure H_2O -vapor heat treatment for improvement of electrical properties. Changes in defect states, potential barrier height and effective carrier dens-

ity following defect reduction are discussed using a numerical analysis program. Structural properties are also investigated using Stokes Raman scattering spectra and X-ray-diffraction measurements.

2 Experimental

Amorphous silicon films with a thickness of 50 nm were formed on quartz-glass substrates by the low-pressure chemical vapor deposition (LPCVD) method. Heat treatment at 600°C for 48 h was carried out for amorphous silicon films in nitrogen atmosphere. Phosphorus atoms were used as dopants at concentrations of $1.1 \times 10^{20} \text{ cm}^{-3}$ and $6.0 \times 10^{18} \text{ cm}^{-3}$ by ion implantation at an energy of 80 keV through a SiO_2 layer with a thickness of 100 nm. Heat treatment at 600°C for 24 h was carried out again for activation of dopant atoms. In order to analyze the free-carrier optical absorption, the optical reflective spectra for $1.1 \times 10^{20} \text{ cm}^{-3}$ -phosphorus-doped samples were measured in the infrared range between 400 cm^{-1} and 4000 cm^{-1} by conventional Fourier transform infrared spectroscopy (FT-IR BOMEM MB-100). Calculated reflective spectra were also obtained by an analysis program of free-carrier optical absorption with parameters of carrier mobility and carrier density [7–13]. Best agreement of experimental and calculated spectra gave the carrier mobility and the carrier density of the free carriers. The carrier mobility and the carrier density of the electrical current for $1.1 \times 10^{20} \text{ cm}^{-3}$ -phosphorus-doped samples were also obtained by Hall-effect current measurements using the Van der Pauw method. For improvement of electrical properties, a 28-ns pulsed XeCl excimer laser with a wavelength of 308 nm was irradiated at a vacuum level of $1 \times 10^{-4} \text{ Pa}$ and room temperature. The laser energy density increased from $160 \text{ mJ}/\text{cm}^2$ to $500 \text{ mJ}/\text{cm}^2$ in $40\text{--}50 \text{ mJ}/\text{cm}^2$ steps with five pulses of irradiation at each energy step. $6.0 \times 10^{18} \text{ cm}^{-3}$ -phosphorus doped samples were used for electrical conductivity measurements. High-pressure H_2O -vapor heat treatment was carried out at 260°C for 3 h in $1.3 \times 10^6 \text{ Pa}$ - H_2O vapor in a pressure-proof stainless chamber [14–16] as well as a laser anneal. Changes in electrical properties were investigated using an analysis program in order to analyze electrically active defect states.

In order to investigate the crystalline volume fraction, Stokes Raman scattering spectra were measured at room tem-

✉ Fax: +42-388-7436, E-mail: tsamesim@cc.tuat.ac.jp

perature. The crystalline volume fraction was estimated with $S_{c-Si}/(S_{c-Si} + S_{a-Si})$, where S_{c-Si} is the integrated scattering intensity of a transverse optical (TO) phonon of crystalline silicon and S_{a-Si} is that of amorphous silicon. Moreover, an X-ray-diffraction measurement was also used to understand structural properties of SPC-poly-Si films.

3 Results and discussion

Figure 1 shows changes in the carrier mobility (a) and the carrier density (b) estimated by analysis of free-carrier optical absorption and Hall-effect current measurement as a function of the laser energy density for $1.1 \times 10^{20} \text{ cm}^{-3}$ -phosphorus-doped solid-phase crystallized polycrystalline silicon (SPC-poly-Si) films. As shown in Fig. 1a, the carrier mobility (μ_{FCA}) estimated by analysis of the free-carrier optical absorption was about $32 \text{ cm}^2/\text{Vs}$ for the initial SPC-poly-Si films, which was close to that of single-crystalline sil-

icon with the heavy phosphorus-doping concentrations [17]. The carrier mobility (μ_{Hall}) obtained by Hall-effect current measurement for the initial SPC-poly-Si films was also as high as about $30 \text{ cm}^2/\text{Vs}$. The values for μ_{FCA} and μ_{Hall} hardly changed with laser annealing at energy densities from $240 \text{ mJ}/\text{cm}^2$ to $500 \text{ mJ}/\text{cm}^2$. The results of Fig. 1a indicate that SPC-poly-Si films have crystalline grains with good electrical properties associated with high mobility and have grain boundaries with low scattering probability. On the other hand, the average carrier densities estimated by analysis of free-carrier optical absorption (N_{FCA}) and Hall-effect current measurement (N_{Hall}) were low for the initial SPC-poly-Si films, as shown in Fig. 1b. The values of N_{FCA} and N_{Hall} for the initial SPC-poly-Si films were $5.0 \times 10^{19} \text{ cm}^{-3}$ and $3.8 \times 10^{19} \text{ cm}^{-3}$, respectively. The values of N_{FCA} and N_{Hall} increased to $1.1 \times 10^{20} \text{ cm}^{-3}$ and $9.6 \times 10^{19} \text{ cm}^{-3}$, respectively, as the laser energy density increased to $500 \text{ mJ}/\text{cm}^2$. This result means that the density of activated dopant atoms was less than half of the density of implanted dopant atoms for the initial SPC-poly-Si films, and that the dopant atoms were almost completely activated by a laser anneal at $500 \text{ mJ}/\text{cm}^2$.

In order to investigate structural properties, Stokes Raman scattering and X-ray-diffraction spectra were measured. Figure 2 shows Stokes Raman scattering spectra for the initial SPC-poly-Si films and films laser-annealed at $300 \text{ mJ}/\text{cm}^2$ and $500 \text{ mJ}/\text{cm}^2$ (a) and the crystalline volume fraction as a function of the laser energy density (b). There was a sharp peak of the crystalline TO phonon around 520 cm^{-1} and a broad band associated with the TO phonons of disordered amorphous silicon bonding in lower wave-number regions than that of the crystalline TO phonon for the initial SPC-poly-Si films as shown in Fig. 2a. A laser anneal increased the intensity of the crystalline TO phonon and reduced the intensity of the TO phonon of disordered amorphous silicon. The crystalline volume fraction was 0.43 for the initial SPC-poly-Si films. It was increased to 0.93 as the laser energy density increased to $500 \text{ mJ}/\text{cm}^2$, as shown in Fig. 2b. Figure 2b also represents the dopant activation ratio, which was the value of the carrier density (measured by the free-carrier optical absorption) divided by the phosphorus-doping concentration ($1.1 \times 10^{20} \text{ cm}^{-3}$). The initial SPC-poly-Si films had a low dopant activation ratio of 0.45. It increased to 0.95 as the laser energy density increased to $500 \text{ mJ}/\text{cm}^2$. There was an agreement between the crystalline volume fraction and the dopant activation ratio.

X-ray-diffraction measurement revealed that the crystalline grains in the initial SPC-poly-Si films mainly had a (111) crystalline orientation normal to the substrate surface. The angle of the (111) orientation was closely distributed within plus or minus one degree around 90 degrees to the substrate surface. The sharp distribution of the (111) angle was kept after laser annealing. Figure 3 shows (111) diffraction spectra as a function of the diffraction angle for the initial SPC-poly-Si films and films laser-annealed at $300 \text{ mJ}/\text{cm}^2$ and $500 \text{ mJ}/\text{cm}^2$. The peak diffraction intensity increased as the laser energy density increased. The amorphous regions existing in the initial films were melted by the laser anneal and probably crystallized epitaxially from the initial crystalline grains in the lateral direction. The grain size was consequently increased by the laser anneal.

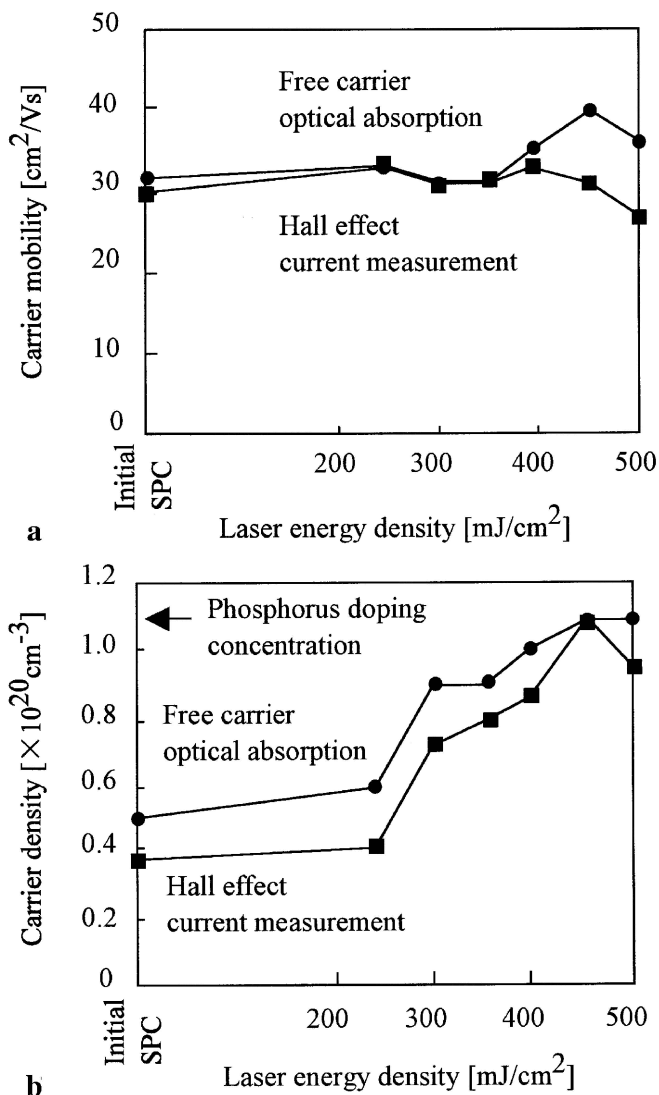
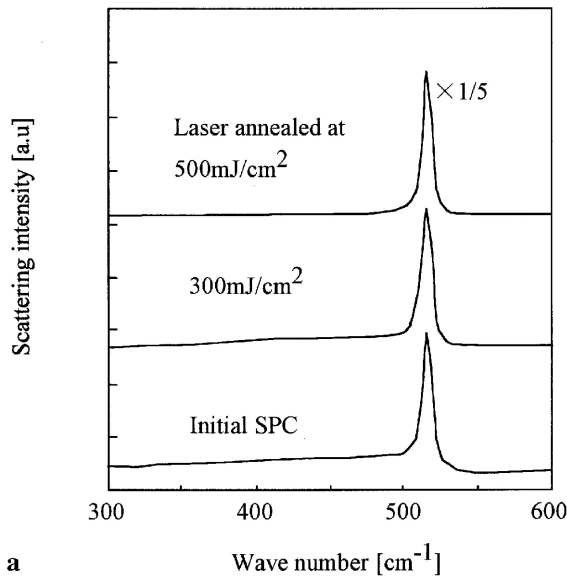
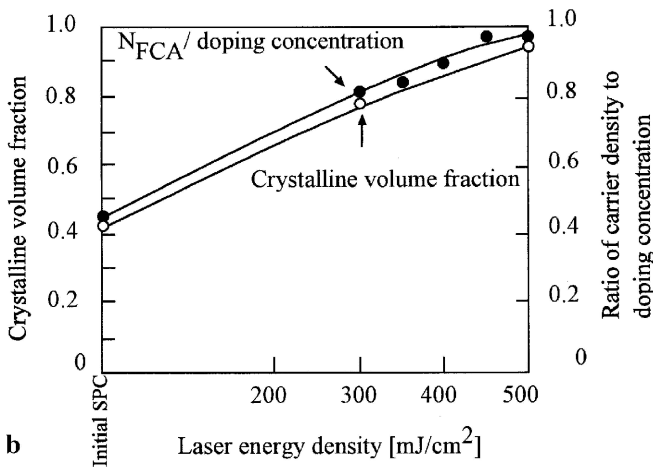


FIGURE 1 Carrier mobility (a) and carrier density (b) obtained by analysis of free-carrier optical absorption and Hall-effect current measurement as a function of the energy density of XeCl excimer laser for $1.1 \times 10^{20} \text{ cm}^{-3}$ -phosphorus-doped 50-nm-thick SPC-poly-Si films



a



b

FIGURE 2 Stokes Raman scattering spectra for 50-nm-thick SPC-poly-Si films, films laser-annealed at 300 mJ/cm² and 500 mJ/cm² (a) and crystalline volume fraction defined by $S_{c-Si}/(S_{c-Si} + S_{a-Si})$ as a function of the laser energy density (b). S_{c-Si} is the integrated scattering intensity of the transverse optical phonon of crystalline silicon and S_{a-Si} is that of amorphous silicon. **b** also shows the ratio of the carrier density (N_{FCA}) obtained by free-carrier optical absorption to the phosphorus-doping concentration ($1.1 \times 10^{20} \text{ cm}^{-3}$) as a function of the laser energy density for $1.1 \times 10^{20} \text{ cm}^{-3}$ -phosphorus-doped 50-nm-thick SPC-poly-Si films

The experimental results of Figs. 1 to 3 indicate the following electrical and structural model for SPC-poly-Si films. The high values of μ_{FCA} and μ_{Hall} mean that the grains have crystalline regions with good electrical properties. On the other hand, N_{FCA} , N_{Hall} and the low crystalline volume fraction mean that there are substantial disordered amorphous regions in the crystalline grains. The high carrier mobility suggested that there were crystalline paths between grain boundaries. Therefore, the amorphous regions were probably isolated in many small domains in the grains. They would reduce the effective width of the carrier transport because of their high resistivity, but would not fatally prevent the carrier transport due to their isolation. The increases of N_{FCA} , N_{Hall} and the crystalline volume fraction by laser annealing mean that the area of the amorphous regions was reduced through laser-induced melt regrowth and the effective width of the carrier

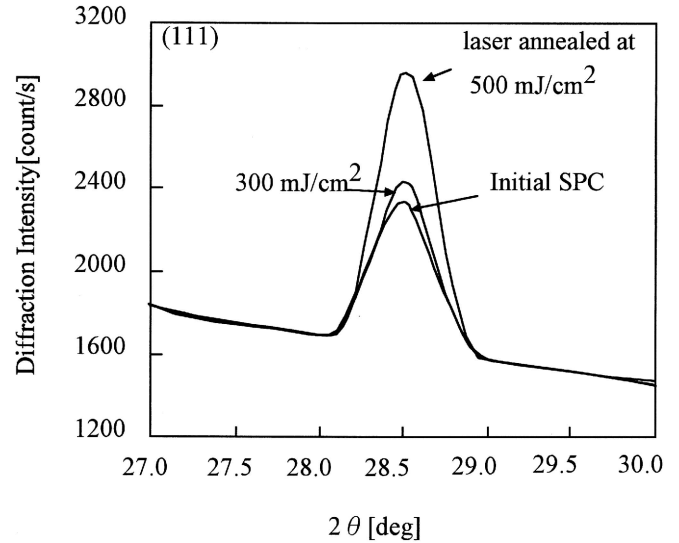


FIGURE 3 X-ray-diffraction intensity spectra of (111)-oriented structure as a function of incident angle for initial 50-nm-thick SPC-poly-Si films and films laser-annealed at 300 mJ/cm² and 500 mJ/cm²

transport increased. The high mobility for initial the SPC-poly-Si films also means that the grain boundaries had a low carrier-scattering probability. The grain boundaries with the low carrier-scattering probability were probably formed between crystalline grains whose crystalline orientation angles had only small differences so-called sub-grain boundaries. X-ray-diffraction measurements showed that most of the crystalline grains were sharply oriented with (111) normal to the substrate surface. We therefore believe that there is a high probability of grain-boundary formation with a small difference of lattice orientation. X-ray measurements showed that this characteristic was maintained after a laser anneal. A laser anneal has the advantage of improvement of structural properties because of reduction of disordered states in crystalline grains. However, it does not improve the carrier mobility because the initial mobility is already high.

In order to investigate electrically active defect states, we analyzed the electrical conductivity for $6.0 \times 10^{18} \text{ cm}^{-3}$ -phosphorus-doped SPC-poly-Si films, because electrical devices such as TFTs operate with carrier densities of 10^{17} – 10^{18} cm^{-3} in their on-states. Figure 4 shows the change in the electrical conductivity as a function of the laser energy density. Although the electrical conductivity was 3.2 S/cm for the initial SPC-poly-Si films, it drastically decreased to $1.7 \times 10^{-2} \text{ S/cm}$ as the laser energy density increased to 500 mJ/cm². As discussed previously, a laser anneal increased the activation ratio of the dopant atoms. The result of Fig. 3 therefore indicates that the laser anneal produced defect states at grain boundaries, which could trap electron carriers. In order to reduce electrically active defect states, a $1.3 \times 10^6 \text{ Pa-H}_2\text{O}$ -vapor heat treatment at 260 °C for 3 h was carried out. Figure 4 also shows the change in the electrical conductivity as a function of laser energy density after such high-pressure H₂O-vapor heat treatment. The electrical conductivity was increased by high-pressure H₂O-vapor heat treatment from 3.2 S/cm to 14.7 S/cm for the initial SPC-poly-Si films. Moreover, after high-pressure H₂O-vapor heat treatment, it increased to 31.3 S/cm as

the laser energy density increased to 500 mJ/cm². The results of Fig. 4 suggest that high-pressure H₂O-vapor heat treatment reduced the density of electrically active defect states for the initial SPC-poly-Si films as well as for laser-annealed SPC-poly-Si films. The electrical conductivity of 31.3 S/cm for the films treated with a laser anneal at 500 mJ/cm² and the high-pressure H₂O-vapor anneal was 10 times higher than that of 3.2 S/cm for the initial SPC-poly-Si films treated with no laser or no high-pressure H₂O-vapor heat treatments. This result shows that the combination of a laser anneal with a high-pressure H₂O-vapor anneal is effective to improve electrical properties of SPC-poly-Si films.

The defect states trapping electron carriers were analyzed using a one-dimensional numerical analysis program with statistical thermodynamics [14, 18–22]. As assumptions of the analysis program, the crystalline region has an energy-band structure of single-crystalline silicon and no defect states. The defect states localize only at grain boundaries. As defect states, the tail-type states caused by a disordered Si bonding network are introduced. The tail states were defined so that the density exponentially decayed from valence- and conduction-band edges to mid-gap. The width of the tail states was defined as 1/e of the peak density of the effective density of states. The Gaussian-type deep-level states caused by Si dangling bonds were also introduced at mid-gap. The width of deep-level states was also defined as 1/e of the peak density. The crystalline volume fraction (X_c) obtained experimentally was introduced as the effective width of the carrier-transport path. Charge neutrality of the whole crystalline grain and the grain boundary is achieved among electron density (n), negatively charged density of states (X_d^-), ionized donor density (N_d^+) and hole density (p) ($n + X_d^- = N_d^+ + p$), which are determined by the Fermi–Dirac statistical distribution function. Free carriers near a grain boundary are trapped by defects localized at the grain boundary; therefore ionized donor atoms near the grain boundary become space charges, which cause potential barriers. The potential barrier

$\Phi(x)$ at point x was determined by the following Poisson's equation:

$$\frac{\partial^2 \Phi(x)}{\partial x^2} = \frac{q(n(x) - Nd^+(x) - p(x))}{\epsilon_0 \epsilon_s},$$

where q is the elemental charge, ϵ_0 is the vacuum dielectric constant and ϵ_s is the specific dielectric constant of silicon. The electron density $n(x)$ at point x in the lateral direction from the mid-point of the crystalline grain is given as

$$n(x) = N_c \exp \left\{ \frac{-q(E_g - E_f + \Phi(x))}{kT} \right\},$$

where N_c is the effective density of states at the conduction-band edge, E_g is the energy-band gap of single-crystalline silicon, E_f is the height of the Fermi level from the valence-band edge at the middle point of the crystalline grain, k is the Boltzmann constant and T is the absolute temperature. The effective electron density n_{eff} is calculated using $n(x)$ and it is expressed as

$$n_{\text{eff}} = X_c \frac{L}{2} \left(\int_0^{L/2} \frac{1}{n(x)} dx \right)^{-1},$$

where X_c is the crystalline volume fraction estimated by Stokes Raman scattering spectra shown in Fig. 2b and L is the average crystalline grain size. The analysis was carried out under the average grain size of 400 nm. The average volume density of electron carriers n_V is also calculated as

$$n_V = X_c \frac{2}{L} \left(\int_0^{L/2} n(x) dx \right).$$

The carrier mobility is calculated with the lattice-vibration scattering and ionized impurity scattering effects [23].

Figure 5 shows experimental and calculated electrical conductivities with different temperatures for the initial SPC-poly-Si films and films laser-annealed at 300 mJ/cm² and 500 mJ/cm². The electrical conductivity for the initial SPC-poly-Si films (a) was increased from 3.2 S/cm to 8.3 S/cm as the temperature increased from room temperature to 200 °C. The electrical conductivity was low at 1.7×10^{-2} S/cm at room temperature for films laser-annealed at 500 mJ/cm² (c), but it markedly increased to 7.7 S/cm as the temperature increased to 200 °C. Figure 5 also shows the change in the electrical conductivity with temperature after high-pressure H₂O-vapor heat treatment. The electrical conductivity was increased to 14.7 S/cm and 31.3 S/cm at room temperature for the initial SPC-poly-Si films (A) and films laser-annealed at 500 mJ/cm² (C). It was increased to 25.7 S/cm and 54.6 S/cm as the temperature increased, respectively, while their increase ratio with temperature was almost the same.

Figure 6 shows the energy distribution of the density of defect states in the Si band gap for the initial SPC-poly-Si

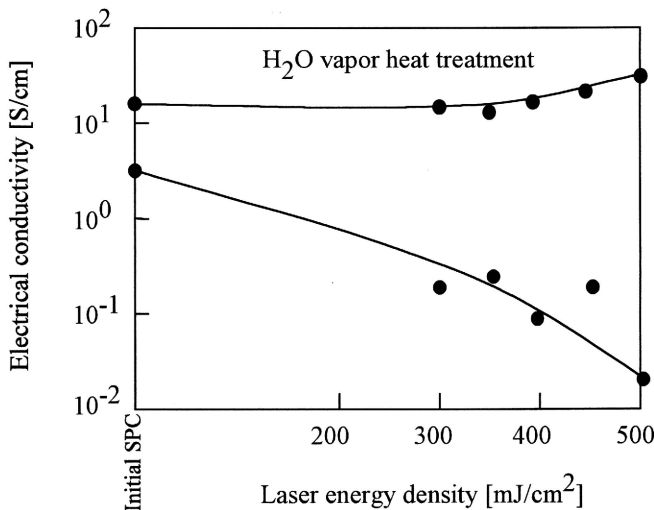


FIGURE 4 Electrical conductivity as a function of laser energy density for 6.0×10^{18} cm⁻³-phosphorus-doped 50-nm-thick SPC-poly-Si films and the electrical conductivity after high-pressure H₂O-vapor heat treatment at 260 °C for 3 h with 1.3×10^6 Pa

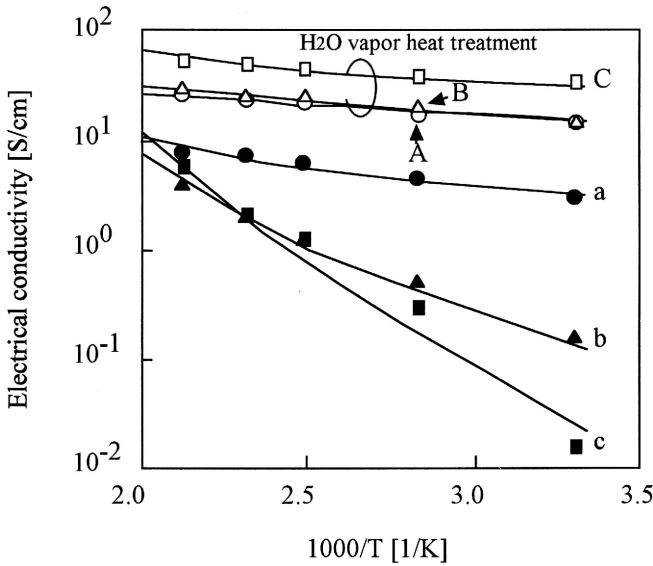


FIGURE 5 Experimental and calculated electrical conductivities as a function of temperature for initial $6.0 \times 10^{18} \text{ cm}^{-3}$ -phosphorus-doped 50-nm-thick SPC-poly-Si films and films laser-annealed at 300 and 500 mJ/cm^2 . Those after high-pressure H_2O -vapor heat treatment at 260 $^\circ\text{C}$ for 3 h with $1.3 \times 10^6 \text{ Pa}$ are also shown. *Solid marks* and *solid curves* represent the experimental and the calculated electrical conductivities. In this figure, “a” shows the initial SPC-poly-Si films and “b” and “c” show the SPC-poly-Si films laser-annealed at 300 mJ/cm^2 and 500 mJ/cm^2 , respectively. “A”, “B” and “C” mean the electrical conductivity after high-pressure H_2O -vapor heat treatment for samples assigned the corresponding small letter. *Solid curves* show the temperature dependence of the calculated electrical conductivity using a one-dimensional numerical analysis program with statistical thermodynamics

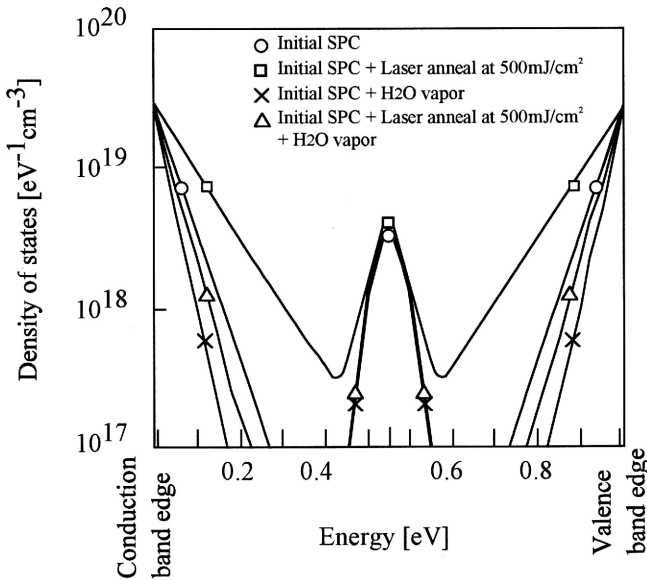


FIGURE 6 Energy distribution of density of states in the silicon band gap obtained by fitting of the calculated conductivity to the experimental conductivity, as shown in Fig. 5

films and films laser-annealed at 500 mJ/cm^2 . The distribution of the density of defect states after high-pressure H_2O -vapor heat treatment is also shown. The initial SPC-poly-Si films have the width of the tail states of 0.05 eV from the band edge and Gaussian-type deep-level states with the width

of 0.10 eV at a peak density of $4.4 \times 10^{18} \text{ eV}^{-1} \text{ cm}^{-3}$. A laser anneal at 500 mJ/cm^2 increased the width of the tail states to 0.10 eV. This indicates that Si bonding networks at grain boundary became much more disordered due to the rapid melting and regrowth process by laser annealing [24, 25]. The density of the deep-level states was almost unchanged. High-pressure H_2O -vapor heat treatment drastically reduced the tail states to 0.03 eV and 0.04 eV for the initial SPC-poly-Si films and films laser-annealed at 500 mJ/cm^2 , respectively. The peak density of the deep-level states was slightly reduced to $3.5 \times 10^{18} \text{ eV}^{-1} \text{ cm}^{-3}$ for each case.

Figure 7 shows the total density of defect states (tail states + deep-level states) (a) and the carrier density (b) as a function of the laser energy density. The total density of defect states for the initial SPC-poly-Si films was estimated as $2.9 \times 10^{18} \text{ cm}^{-3}$. It increased to $6.2 \times 10^{18} \text{ cm}^{-3}$ as the laser energy density increased to 500 mJ/cm^2 . The increase of the total density of defect states results in an increase of the potential barrier height from 0.17 eV to 0.32 eV, as repre-

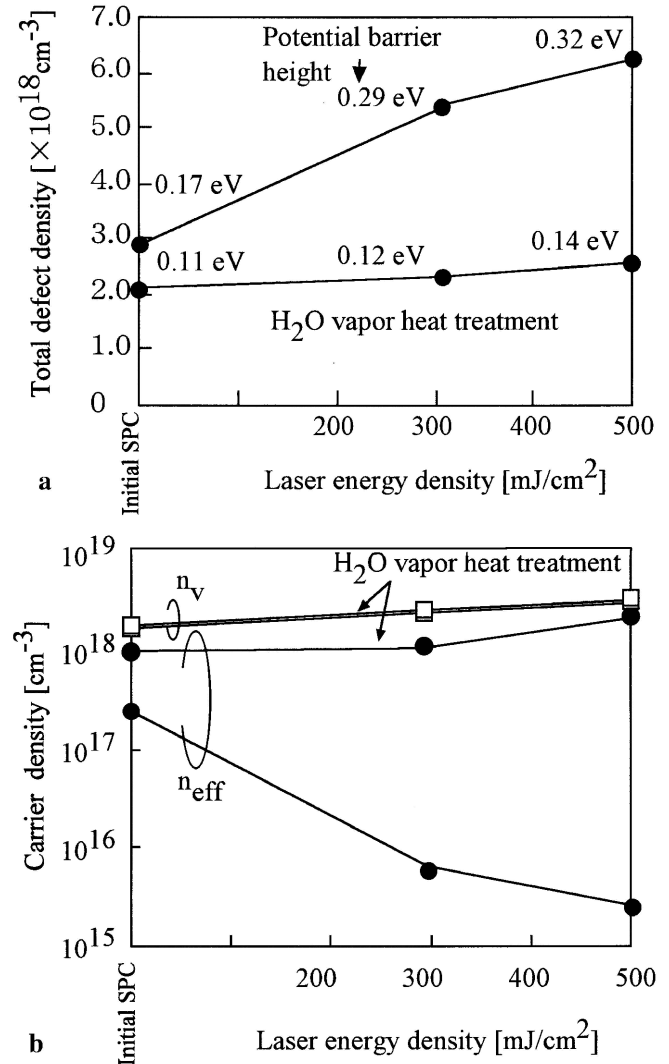


FIGURE 7 Total density of defect states (a) and carrier density (b) as a function of the laser energy density. The potential barrier height is presented in a. The effective carrier density (n_{eff}) and the average volume density of electron carriers (n_V) are presented in b

sented in Fig. 7a. The increase of the potential barrier height markedly reduced the effective carrier density (n_{eff}) from $2.8 \times 10^{17} \text{ cm}^{-3}$ to $2.8 \times 10^{15} \text{ cm}^{-3}$ as the laser energy density increased for $6.0 \times 10^{18} \text{ cm}^{-3}$ -phosphorus-doped SPC-poly-Si films, as shown in Fig. 7b, due to the expansion of the depletion region from 15-nm to 20-nm thick around the grain boundaries. On the other hand, the analysis of the electrical conductivity also gave the average volume density of electron carriers. This density was high at $1.6 \times 10^{18} \text{ cm}^{-3}$ for the initial SPC-poly-Si films. It increased to $3.3 \times 10^{18} \text{ cm}^{-3}$ as the laser energy density increased because the crystalline volume fraction increased. The potential barrier at grain boundaries blocked carrier transport between conductive crystalline grains. After high-pressure H_2O -vapor heat treatment, the total density of defect states decreased to $2.1 \times 10^{18} \text{ cm}^{-3}$ and $2.6 \times 10^{18} \text{ cm}^{-3}$ as well as a decrease of the potential barrier height of 0.11 eV and 0.14 eV for the initial SPC-poly-Si films and films laser-annealed at 500 mJ/cm^2 , respectively, as shown in Fig. 7a. The effective carrier density therefore increased from $1.0 \times 10^{18} \text{ cm}^{-3}$ to $2.2 \times 10^{18} \text{ cm}^{-3}$ as the laser energy density increased after high-pressure H_2O -vapor heat treatment, as shown in Fig. 7b. On the other hand, the average volume density of electron carriers n_V was almost unchanged with high-pressure H_2O -vapor heat treatment for the initial and laser-annealed samples, because most of the regions in the crystalline grains were conductive and the depletion regions just around the grain boundaries were reduced by H_2O -vapor heat treatment. The effective carrier density was consequently increased from $2.8 \times 10^{17} \text{ cm}^{-3}$ to $2.2 \times 10^{18} \text{ cm}^{-3}$ by combination of a laser anneal with a high-pressure H_2O -vapor heat treatment because of the increased crystalline volume fraction as well as reduction of the density of defect states.

4 Summary

We investigated electrical and structural properties of solid-phase crystallized polycrystalline silicon (SPC-poly-Si) films fabricated at 600°C for 48 h. The carrier mobilities estimated by analysis of free-carrier optical absorption and Hall-effect current measurement were $32 \text{ cm}^2/\text{Vs}$ and $30 \text{ cm}^2/\text{Vs}$ for $1.1 \times 10^{20} \text{ cm}^{-3}$ -phosphorus-doped SPC-poly-Si films. The SPC-poly-Si films have good electrical properties with a low carrier-scattering probability at grain boundaries. The carrier density was increased to the doping concentration by a laser anneal. The increase of the carrier density was caused by the reduction of amorphous regions, which was confirmed as an increase of the crystalline volume fraction estimated by Stokes Raman scattering spectra. X-ray-diffraction measurement indicated a strong (111) orientation normal to the substrate surface and that the grain size increased by a laser anneal at 500 mJ/cm^2 . The electrical conductivity decreased from 3.2 S/cm to $1.7 \times 10^{-2} \text{ S/cm}$ as the laser energy density increased to

500 mJ/cm^2 for $6.0 \times 10^{18} \text{ cm}^{-3}$ -phosphorus-doped SPC-poly-Si films because of formation of the defect states at grain boundaries. The total density of defect states increased from $2.9 \times 10^{18} \text{ cm}^{-3}$ (initial) to $6.2 \times 10^{18} \text{ cm}^{-3}$ by a laser anneal at 500 mJ/cm^2 . The effective carrier density was drastically reduced from $2.8 \times 10^{17} \text{ cm}^{-3}$ to $2.8 \times 10^{15} \text{ cm}^{-3}$. On the other hand, the electrical conductivity was increased to 31.3 S/cm by a laser anneal at 500 mJ/cm^2 and an additional high-pressure H_2O -vapor heat treatment. The total density of defect states was reduced to $2.6 \times 10^{18} \text{ cm}^{-3}$. The effective carrier density was increased to $2.2 \times 10^{18} \text{ cm}^{-3}$. The combination of a laser anneal with a high-pressure H_2O -vapor heat treatment is effective for improvement of electrical properties of SPC-poly-Si films because of an increase of the crystalline volume fraction as well as a reduction of the density of defect states.

REFERENCES

- 1 C.H. Hong, C.Y. Park: J. Appl. Phys. **71**, 5427 (1992)
- 2 J.K. Kim, J.Y. Lee, K.S. Nam: J. Appl. Phys. **77**, 95 (1995)
- 3 T. Noma, T. Yonehara, H. Kumomi: J. Appl. Phys. Lett. **59**, 653 (1991)
- 4 T.W. Little, K. Takahara, H. Koike, T. Nakazawa, I. Yudasaka, H. Ohshima: Jpn. J. Appl. Phys. **30**, 3724 (1991)
- 5 M. Miyasaka, M. Hogyoku, S. Inoue, T. Shimada, J. Stoemenos: in Dig. Tech. Pap. 1999 Int. Workshop Active Matrix Liquid-Cryst. Disp. (Tokyo, Japan 1999), p. 257
- 6 M. Miyasaka, J. Stoemenos: J. Appl. Phys. **86**, 5556 (1999)
- 7 H. Engstrom: J. Appl. Phys. **51**, 5245 (1980)
- 8 M. Born, E. Wolf: *Principles of Optics* (Pergamon, New York 1974) Chaps. 1 and 13
- 9 T. Sameshima, K. Saitoh, N. Aoyama, S. Higashi, M. Kondo, A. Matsuda: Jpn. J. Appl. Phys. **38**, 1892 (1999)
- 10 T. Sameshima, K. Saitoh, M. Sato, A. Tajima, N. Takashima: Jpn. J. Appl. Phys. Lett. **36**, 1360 (1997)
- 11 T. Sameshima: Mater. Res. Soc. Symp. Proc. **536**, 427 (1999)
- 12 T. Sameshima, K. Saitoh, N. Aoyama, M. Tanda, M. Kondo, A. Matsuda, S. Higashi: in Tech. Dig. Int. Photovoltaic Sol. Energy Conf. (Sapporo, Japan 1999), p. 211
- 13 T. Kamiya, T. Nakahata, T. Sameshima, T. Watanabe, T. Mohri: J. Appl. Phys. **88**, 3310 (2000)
- 14 K. Asada, K. Sakamoto, T. Watanabe, T. Sameshima, S. Higashi: Jpn. J. Appl. Phys. **39**, 3882 (2000)
- 15 T. Sameshima, M. Satoh, K. Sakamoto, A. Hisamatsu, K. Ozaki: Jpn. J. Appl. Phys. **37**, 112 (1998)
- 16 T. Sameshima, M. Satoh, K. Sakamoto, K. Ozaki, K. Saitoh: Jpn. J. Appl. Phys. **37**, 4254 (1998)
- 17 E.M. Conwell: Proc. IRE **46**, 1281 (1958)
- 18 Y. Tsunoda, T. Sameshima, S. Higashi: Jpn. J. Appl. Phys. **39**, 1656 (2000)
- 19 J.Y.W. Seto: J. Appl. Phys. **46**, 5247 (1975)
- 20 W.B. Jackson, N.M. Johnson, D.K. Biegelsen: Appl. Phys. Lett. **43**, 195 (1983)
- 21 M. Kimura, R. Nozawa, S. Inoue, T. Shimoda, B.O.-K. Lui, S.W.-B. Tam, P. Migliorato: Jpn. J. Appl. Phys. **40**, 318 (2001)
- 22 S. Higashi, K. Ozaki, K. Sakamoto, Y. Kano, T. Sameshima: Jpn. J. Appl. Phys. **38**, 857 (1999)
- 23 C. Jacoboni, C. Canali, G. Ottaviani, A. Alberigi Quaranta: Solid State Electron. **20**, 77 (1977)
- 24 T. Sameshima, M. Hara, S. Usui: Jpn. J. Appl. Phys. **28**, 1789 (1989)
- 25 T. Sameshima: Appl. Surf. Sci. **96-98**, 352 (1996)